



Pb²⁺ removal performance by cotton-based and magnetic modified cotton-based biochar prepared from agricultural waste biomass

Yanling Zou^{a,b,†}, Fei Xu^{a,†}, Qiang Kong^{a,c}, Dawei Shang^{a,b}, Yujia Zhang^d, Wenhan Guo^a, Qian Wang^a, Congcong Zhao^a, Yuanda Du^{a,*}

^aCollege of Geography and Environment, Collaborative Innovation Center of Human-Nature and Green Development in Universities of Shandong, Shandong Normal University, Jinan 250014, China, Tel. +86 531 86182550; Fax: +86 531 86180107; emails: yddu@sdsu.edu.cn (Y. Du), 1156433265@qq.com (Y. Zou), xufeiadnu@yahoo.com (F. Xu), kongqiang0531@hotmail.com (Q. Kong), 1120953792@qq.com (D. Shang), 793290917@qq.com (W. Guo), qianwang86@sdsu.edu.cn (Q. Wang), zhaocongcong1009@163.com (C. Zhao)

^bInstitute of Environment and Ecology, Shandong Normal University, Jinan 250014, China

^cDepartment of Civil and Environmental Engineering, National University of Singapore, 117576 Singapore, Singapore

^dCollege of Life Science, Shandong Normal University, Jinan 250014, China, email: 1370483013@qq.com (Y. Zhang)

Received 26 March 2020; Accepted 3 August 2020

ABSTRACT

This study aimed to investigate the Pb²⁺ removal performance of cotton-based biochar (CB) and magnetic modified cotton-based biochar (MCB). The scanning electron microscopy revealed that MCB exhibiting a porous honeycomb structure with a specific surface area of 613.69 m²/g which bigger than that of CB (356.68 m²/g). The Fourier transform infrared spectrum analysis indicated the presence of metal oxides and hydroxides in MCB and the functional groups of O–H, C=O, and C≡C in both MCB and CB. The signal of Fe₃O₄ and Fe₃C was observed in X-ray diffraction analysis of MCB, which indicated the success of magnetic modification of MCB. The maximum monolayer adsorption capacities (Q_m) of MCB and CB on Pb²⁺ were 208.33 and 156.25 mg/g, respectively. The adsorption kinetics of MCB and CB were both best fitted with the pseudo-second-order model ($R^2 > 0.99$), and the adsorption isotherms of the two biochar were well-described by the Langmuir adsorption model ($R^2 > 0.99$). The results of this study revealed the significant physicochemical difference of two biochar and indicated that magnetic modification can enhance the Pb²⁺ adsorption capacity of biochar, suggesting that MCB is a potential adsorbent for wastewater treatment.

Keywords: Biochar; Magnetic modified; Lead removal; Adsorption

1. Introduction

Lead (Pb²⁺) is one of the predominant heavy metal byproducts of industrial production. There are multiple wastewater discharge sources of lead into aquatic and terrestrial environments, namely: lead smelting, lead battery manufacturing, pigment fabrication, and various metallurgical industries [1–6]. Based on environmental research and epidemiological analysis, environmental exposure to lead has been identified as a major risk factor for the ecosystem

and human health [7]. Lead can enter the human body through the skin, digestive tract, and respiratory system, to accumulate in various organs and tissues due to its low metabolic degradation [8,9]. Excessive lead content in the human body can cause damage to biochemical systems and result in various medical ailments, including renal failure, anemia, and neurological disorders [10–13]. Considering the ecological and health impacts of lead, specific standards and legislation were corroborated to establish permitted lead levels in water sources and drinking water. Currently, the

* Corresponding author.

† These authors have contributed equally to this works.

World Health Organization (WHO) permits up to 10 µg/L of lead in water, and the maximum permitted lead concentrations in surface water for the European Union (EU), USA, and China are 10, 15, and 10 µg/L, respectively [14,15].

During recent decades, several technologies were developed for lead removal including coagulation, chemical precipitation, solvent extraction, ion exchange, electrolysis, membrane separation, permeable reactive barriers, and electro dialysis [8,16–19]. Despite their many advantages, the application of these technologies was limited due to a variety of factors, such as massive consumption of reagents, destabilization of removal performance, generation of toxic sludge, and escalating costs [20].

Biochar is a class of biomass-based materials that are characterized by a porous carbonaceous structure and the presence of diverse surface functional groups [21,22]. It is considered as a promising adsorbent of various contaminants due to its effective adsorption rate and low ecological cost [23]. The high adsorption capacity of biochar for pollutants is facilitated by its large surface area, high pore size volume, and plentiful functional groups [24]. Previous study indicated that biochar has significant potential for the removal of heavy metals from aqueous solutions [25]. Zhou et al. [26] showed the chitosan-modified biochar could effectively remove Pb²⁺, Cu²⁺, and Cd²⁺ from the aqueous solution, Saleh et al. [27] reported that the removal efficiency of the magnetic activated carbon/tungsten nanocomposite with aluminum in aquatic environments was 90%, and Shan et al. [28] showed that the single and competitive adsorption affinity of peanut shell-derived biochar to heavy metals.

Due to the small particle size, the powdered biochar can well disperse in aqueous solution which makes it difficult to separate during its practical application [29]. Introducing a magnetic medium (e.g., magnetite, γ-Fe₂O₃) to the biochar by chemical modification is an efficient method to enable the sorbent to be effectively separated by magnetic separating technique [30,31]. In addition, the magnetic media can enhance the removal efficiency of the magnetic sorbents by increasing the adsorption affinity of multiple chemicals [32]. Subedi et al. [33] reported that the maximum adsorption capacity of magnetic chitosan on Cr(VI) was 142.32 mg/g. Imran et al. [34] reported that the maximum Cd²⁺ adsorption of siltstone associated with biochar and magnetite nanoparticles was 117.38 mg/L. Mohan et al. [35] showed that magnetic carbon effectively removed 97% of 2,4,6-trinitrophenol. The above-mentioned data provide essential information for future applications of magnetic biochar in wastewater treatment practices.

An additional benefit is that the feedstock of biochar comes from various waste biomass, such as rice husks, peanut shells, cotton stalks, wheat stalks, and macroalgae [36–39]. The efficient utilization of agricultural wastes is an important approach to sustainable agricultural production. Compared with agricultural wastes such as corn straw and wheat straw, the high lignin, and bast fiber content make the cotton straw difficult to recycle effectively [40]. According to literature, biochar fabrication was considered as a potential utilization method of cotton straw, for example, cotton-straw based biochar can remove the As(V) and ofloxacin from aqueous solution [41,42]. Moreover, the magnetization of cotton straw biochar has been rarely reported,

in this study, magnetic cotton-based biochar was investigated with respect to lead removal.

This study aimed to investigate the difference in Pb²⁺ removal performance between cotton-based biochar (CB) and magnetic modified cotton-based biochar (MCB). Scanning electron microscopy (SEM), the Brunauer–Emmett–Teller method (BET), Fourier transform infrared (FTIR) spectroscopy, and X-ray diffraction (XRD) were used to analyze the structural characteristics and chemical traits of the two biochar. The adsorption kinetics, thermodynamics, isotherms, and optimal adsorption conditions were also investigated. The results and knowledge gained from this study contribute to the future application of heavy metal pollution restoration and the efficient and sustainable recycling of agricultural waste.

2. Materials and methods

2.1. Biochar preparation

2.1.1. Preparation of CB

The raw material used in this study was *Gossypium hirsutum* (upland cotton), collected from Liaocheng, China. The cotton stalk was broken into 2 mm fragments using a high-speed grinder (HCP-100, Jinsui Company, China), and subsequently dried at 110°C for 24 h. The CB was carbonized in two stages in a muffle furnace. During the first stage, the temperature was increased from room temperature to 300°C for 1 h. In the second stage, the temperature was increased to 750°C and stabilized for 1.5 h. After cooling to room temperature, the biochar was washed with deionized water to neutral and sifted through 200-mesh once dried, and finally stored.

2.1.2. Preparation of MCB

Cotton stalks, in 2 mm fragments, were impregnated with solutions of K₂CO₃ and Fe₃O₄. According to 25 groups of pilot experiments, the ratio of cotton stalk, K₂CO₃ and Fe₃O₄ were determined as 10:4:0.4 (g/g), then the stalks were dried at 110°C for 24 h. The carbonation process and subsequent treatment of MCB were same to that described earlier for CB.

2.2. Adsorption experiment

The two types of biochar were mixed with 50 mL of Pb²⁺ solution in 100 mL conical flasks and stirred in a concussion incubator for 6 h at 180 rpm. After filtration, the Pb²⁺ content in the filtrate was measured using the xylenol-orange method. All experiments were performed in triplicate to ensure accuracy.

2.3. Biochar characterization

The weight loss of the carbonation process was measured using a thermogravimetric analyzer (TGAQ50, TA Instruments, USA). The temperature was increased from 10°C to 800°C at a rate of 10°C/min in an N₂ atmosphere. The structural properties of MCB and CB were observed by SEM (SUPRA 55, Zeiss Company, Germany). The specific surface area and pore size distribution were measured by the BET

method (Quantachrome, USA). FTIR (Thermo Scientific, USA) was used to analyze the surface functional groups in the wavenumber range of 4,000–500 cm^{-1} . X ray diffractometer (XRD, Japan, SmartLab) recorded the crystallinity and phase of samples. The zeta potential (ZP) was measured using Zeta Plus (New York, USA).

2.4. Batch experiments

Batch experiments were conducted to determine the optimum conditions for removal of Pb^{2+} from the aqueous solution. This study investigated the effects of contact time (0–720 min), temperature (288–308 K), initial concentration (Pb^{2+}) (10–300 mg/L), dosage (0.2–1.6 g/L), and initial pH (1–6) on adsorption. The equation for determining the adsorption quantity is detailed in the supplementary methods section.

2.5. Adsorption kinetics

The adsorption kinetics were studied to determine the kinetic parameters and adsorption mechanism of the two biochar types. The Pb^{2+} solution was mixed with either 1 g/L of MCB or CB at initial concentrations of 100, 200, and 300 mg/L, and then tested at various time intervals (10, 30, 60, 90, 120, 180, 240, 300, 360, 480, 600, and 720 min). The kinetics data were investigated by applying the pseudo-first-order, pseudo-second-order, and diffusion equation models. Please refer to the supplementary methods section for the formula of the kinetic model.

2.6. Adsorption isotherms

The adsorption isotherm was used to determine the adsorption mechanism and heterogeneity of the adsorbent material. The Langmuir, Freundlich, and Dubinin–Radushkevich models were applied to describe the adsorption process in solutions with Pb^{2+} concentrations (10–300 mg/L), temperatures of 288, 298, and 308 K, and when the dosage of MCB or CB was 1 g/L. The adsorption isotherm model formula is shown in the supplementary methods section.

2.7. Adsorption thermodynamics

The adsorption thermodynamics of MCB and CB were evaluated using the Gibbs free energy (ΔG°), enthalpy change (ΔH°), and entropy (ΔS°). The thermodynamic coefficients were determined by the formula shown in the supplementary methods section.

3. Results and discussion

3.1. Characterization of CB and MCB

The TG/DTG curves describe the weight loss in the carbonation process under the N_2 atmosphere. As shown in Fig. 1, weightlessness was divided into three stages at the temperature range of 30°C–900°C. The first stage of mass loss was observed at 30°C–100°C, and the first maximum weight loss of MCB and CB occurred at 30°C and 60°C, due to the predominance of water resulting from evaporation and dehydration

reactions [43]. The second weight loss of MCB and CB was observed at 200°C–600°C and at 200°C–400°C, owing to the thermal decomposition of hemicellulose, cellulose, and lignin (200°C–300°C, 250°C–400°C, and 160°C–900°C, respectively) [44,45]. The third stage of weight loss was evident only in MCB, and occurred at 600°C–800°C. This was due to the further decomposition of lignin and K_2CO_3 , the reduction of Fe_3O_4 , and the generation of intermediate products [46,47].

The surface properties of MCB and CB were observed using SEM. Fig. 2a shows that the surface of the MCB before adsorption was rough and abundant in honeycomb pore structures, whereas the surface of CB (Fig. 2c) was relatively smooth, without significant pores. After adsorption, the active site of MCB (Fig. 2b) was mostly occupied by Pb^{2+} , and the pore structure of CB (Fig. 2d) slightly change, indicating that the pore structure participated in the adsorption process. The SEM results suggest that MCB, with a larger pore structure, had a higher specific surface area and therefore better adsorption capacity than CB.

The pore size distributions of MCB and CB were bifurcated into two prominent parts, as shown in Fig. 3a. The aperture of MCB was mainly distributed in the range of 2–50 nm, indicating a dominantly mesoporous surface, with micropores (0–2 nm) was less evident. The pore size range of CB was 2–50 nm, similar to the mesoporous MCB. The specific surface areas of MCB and CB were calculated as 613.69 and 356.68 m^2/g respectively. These were consistent with the developed surface porosity structure of MCB observed by SEM. The maximum specific surface area of MCB was higher than some other adsorbents, such as; $\text{CeO}_2\text{-MoS}_2$ hybrid magnetic biochar (127.6 m^2/g) [48], wheat straw magnetic biochar (44.31 m^2/g) [49], and KMnO_4 modified magnetic rice husk biochar (275 m^2/g) [50]. As shown in Fig. 3b, the N_2 adsorption–desorption isotherms of MCB and CB were characterized by a mixture of types I and IV. With the combination of type I and IV, the gas adsorption capacity increased rapidly, with an increase in pressure at low values, until the maximum volume adsorbed was reached [39]. The hysteresis ring was observed as a result of the capillary condensation of a high proportion of mesopores, which played a crucial role during the adsorption process [51].

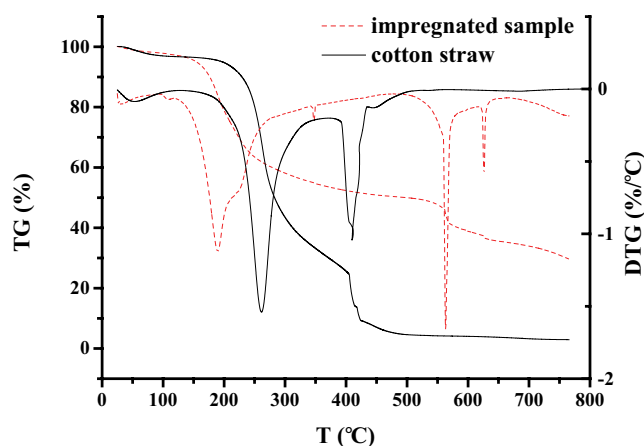


Fig. 1. TG/DTG curves of cotton straw and impregnated sample.

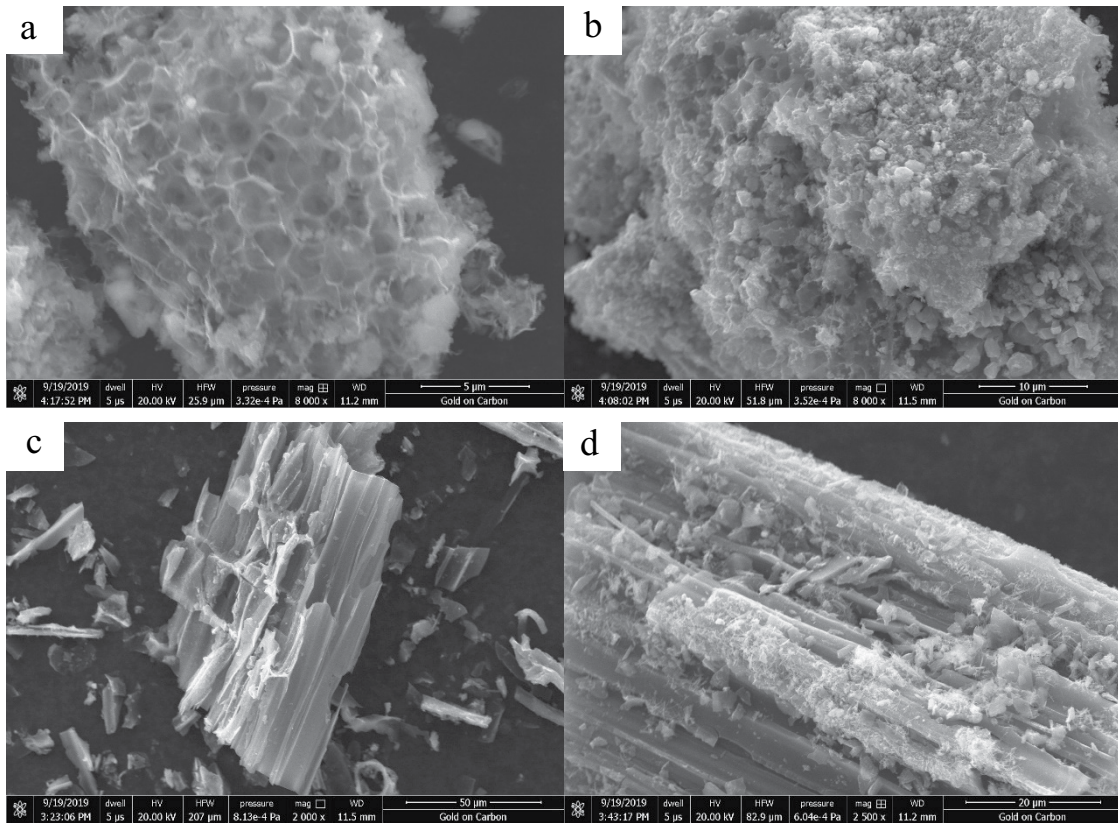


Fig. 2. SEM of MCB and CB (a) MCB before adsorption of Pb^{2+} , (b) MCB after adsorption of Pb^{2+} , (c) CB before adsorption of Pb^{2+} , and (d) CB after adsorption of Pb^{2+} .

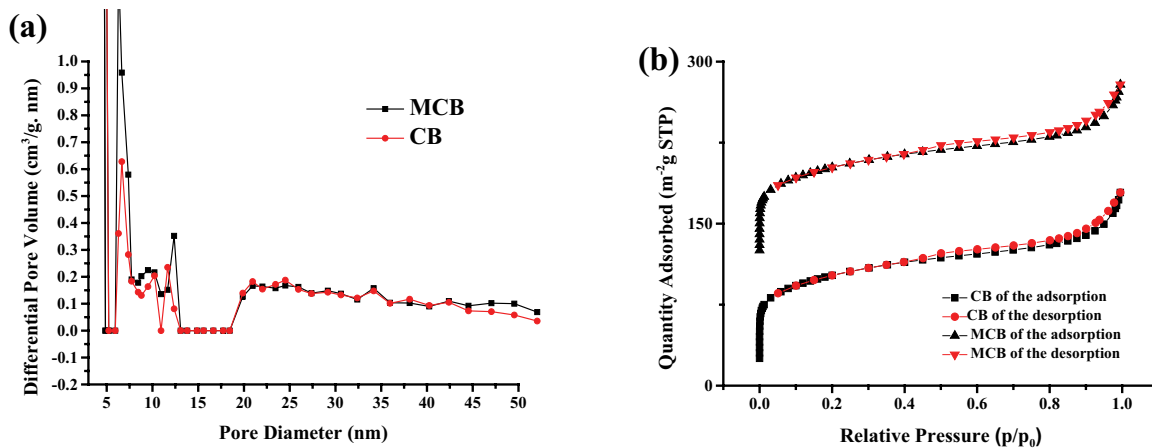


Fig. 3. (a) Pore size distribution of MCB and CB and (b) N_2 adsorption–desorption isotherms of MCB and CB.

The surface functional groups of MCB and CB were analyzed by FTIR spectroscopy. As shown in Fig. 4a, significant peaks at 500–600 cm^{-1} were observed in MCB attributed to the metal-oxygen and metal-hydroxyl vibrations [52,53]. High similarity of peak patterns was observed in the two biochar. The peaks at 3,500–3,700 cm^{-1} indicated the hydroxyl (O–H) groups [54–56]. The peaks at around 2,100–2,400 cm^{-1} were related to deformation vibrations or carbon dioxide in the $C\equiv C$ plane [54,57]. The peak at 1,560 cm^{-1} was indicated by

the $C=O$ and $C=C$ olefinic bonds. After adsorption (Fig. 4b), a CB peak at 2,870 cm^{-1} was identified as the stretching of C–H [58]. The peak intensity decreased in both biochar due to the interactions of the functional groups and lead ions, as well as the shielding effect of the adsorbed molecules. These results indicated that the functional groups of MCB and CB were involved in the adsorption process of Pb^{2+} .

XRD analysis was used to further characterize the chemical profiles of MCB and CB. As shown in Fig. 5, a significant

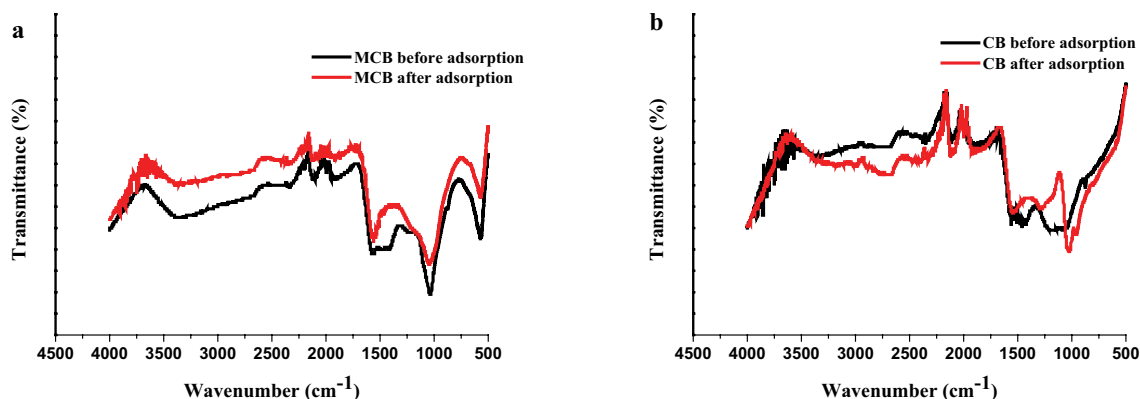


Fig. 4. FTIR spectra of the biochar before and after the adsorption of Pb^{2+} (a) MCB and (b) CB.

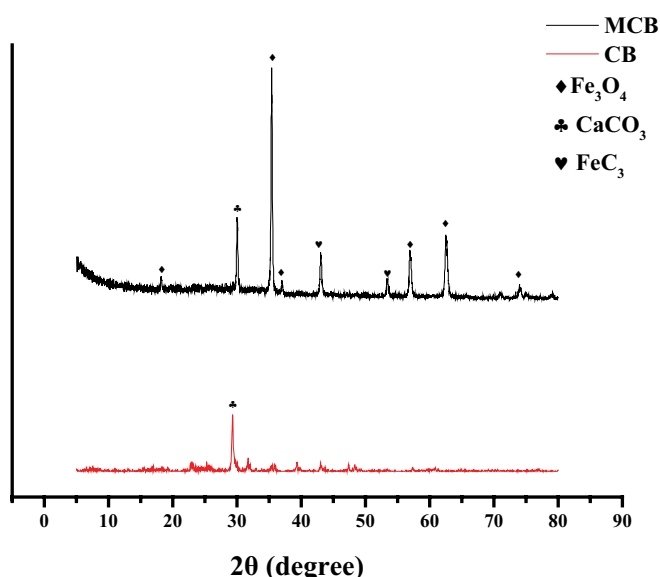


Fig. 5. XRD patterns of MCB and CB.

peak of $CaCO_3$ appeared in both MCB and CB at 29° , as the biochar was washed with deionized water, instead of acid, after carbonation [59]. The diffraction peaks at 35° , 44° , and 57° verified the presence of Fe_3O_4 and Fe_3C . Previous study illustrated that magnetic modification can change the chemical composition of the biochar [60]. The results of XRD analysis combined with the significant difference of two biochar with the respect of physicochemical properties including structure, specific surface area, and lead adsorption performance which indicated the formation of the magnetic biochar. Additionally, one-step method was employed to produce magnetic biochar in some studies, for instance, Lu et al. [61] showed that the magnetic algal carbon/sulfidated nanoscale zerovalent iron composites can efficiently remove of bromated and Zhang et al. [62] revealed the *in-situ* reduction of tetrabromobisphenol A induced by the magnetic seaweed biochar/sulfidated Fe^0 composite. The results of this study indicated the effectiveness of one-step method during the fabrication of magnetic biochar.

Results from the ZP analysis is shown in Fig. 6. The isoelectric points (pI) of MCB and CB were approximately 2.3 and 1 respectively, indicated by the ZP of zero. The measurement of ZP is important to know the nature of the adsorbent under different pH [63]. When the pH value was less than pI, the surface charge of the MCB was positive (due to the protonation reaction). As the pH value was higher than pI, the surface charge of the biochar was negative. This was due to the hydroxy bonding ($-OH$) adsorption under high pH conditions [64–66]. Considering that lead ions are a type of positive ion, the initial pH, (which was higher than pI) could contribute to the improvement of the adsorption capacity.

3.2. Effect of adsorbent dosage

Adsorbent dosage is an important parameter for the optimization of the adsorption process. The effect of MCB and CB dosage on Pb^{2+} removal is shown in Fig. 7. When the biochar dosage increased from 0.2 to 1.6 g/L, the removal rate increased from 55.87% to 100%, and the adsorption quantity decreased from 271.95 to 57.70 mg/g. The adsorption quantity of CB decreased from 176.65 to 58.67 mg/g and removal rate increased from 52% to 96%. According to the adsorption equilibrium formula, under a constant concentration of lead ions, the adsorption capacity of biochar in unit weight decreased gradually with increasing dosage [67]. When the dosage was 0.05 g (1 g/L), the Pb^{2+} removal rates of both MCB and CB approached 90%. Therefore, 0.05 g (1 g/L) was used in the subsequent experiment.

3.3. Effect of initial solution pH

The pH value of the solution can affect the surface charge as well as the ionization degree, and therefore also affect the adsorption ability of the adsorbent. The presence of excessive H^+ or OH^- ions in the solution may change the surface charge characteristics of biochar, considering that Pb^{2+} were positive ion, the high pH could contribute to the improvement of Pb^{2+} removal performance [68]. The effects of solution pH on Pb^{2+} removal by MCB and CB are shown in Fig. 8. When the pH value was above 3.0, the MCB of Pb^{2+} removal rate rapidly increased from 88% to 100%, and the removal rate of CB reached 87%. This result was

consistent with the analysis of the ZP. When the pH value was smaller than the isoelectric point of biochar, the positive charge of biochar led to the electrostatic repulsion of Pb^{2+} . Moreover, the presence of substantial hydrogen ions (H^+) could compete with Pb^{2+} for adsorption sites, leading to a decrease in the removal rate and adsorption performance [69]. When the pH was greater than the isoelectric point, the negative charge of the MCB surface and the concentration of H^+ decreased with increasing pH, and the removal rate and adsorption performance of biochar with Pb^{2+} was enhanced due to the availability of adsorption sites and ionic reactions.

3.4. Effect of contact time

Fig. 9 shows the effect of the contact time of MCB and CB on the adsorption of Pb^{2+} . The removal efficiency of MCB and CB increased rapidly in 0–60 min, with the MCB removal rate increasing from 62% to 87% and CB increasing from 61% to 72%. The removal rate gradually increased

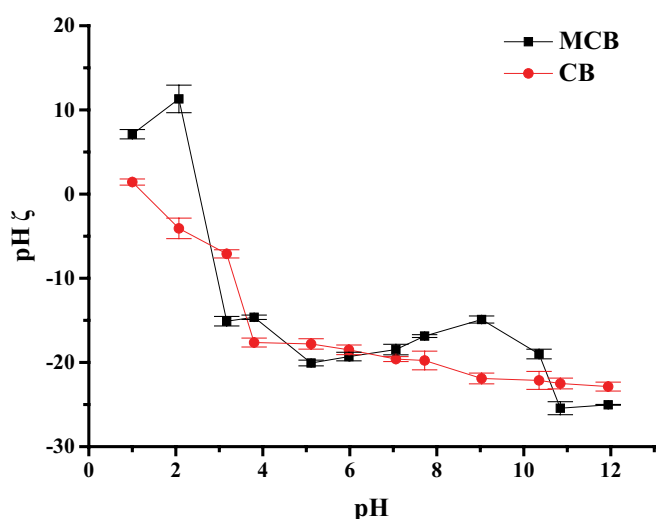


Fig. 6. Zeta potential of MCB and CB under different pH value.

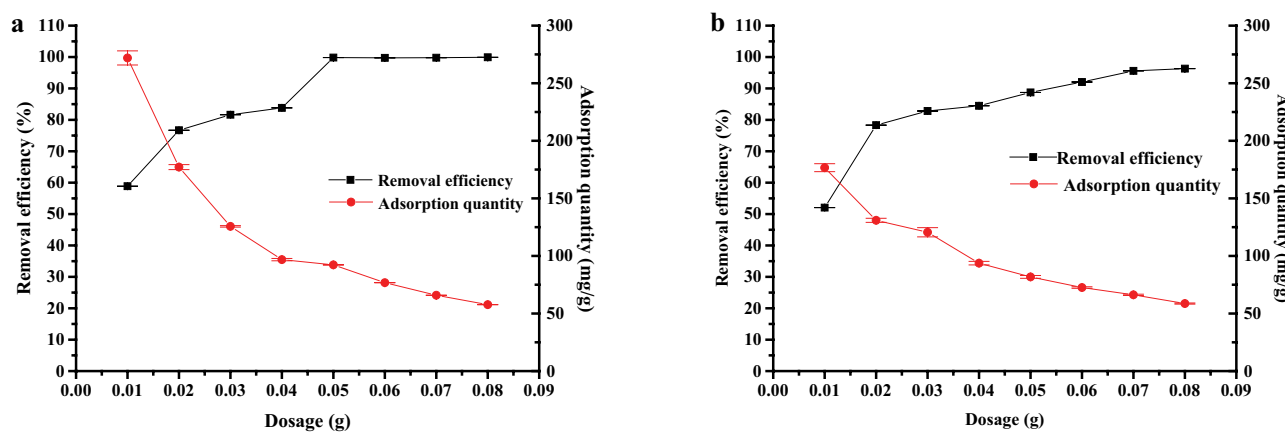


Fig. 7. Effect of dosage on the removal efficiency and adsorption capacity of Pb^{2+} . (a) MCB and (b) CB (initial Pb^{2+} concentration: 100 mg/L; temperature: 298 K; time: 6 h; initial pH: 5).

from 60 to 360 min and then stabilized. At the initial stage of the adsorption process, a high adsorption rate was obtained due to the availability of adsorption sites on the surface of biochar. The removal efficiency increased slowly in the time range of 120–360 min, indicating a decrease in available adsorption sites [70]. The removal rate and adsorption efficiency showed a relatively stable state in contact times of 360–720 min, indicating that the lead ions adsorbed by MCB and CB reached equilibrium owing to surface adsorption saturation [71]. Based on these results, the optimal contact time for Pb^{2+} removal was 360 min.

3.5. Effect of the initial concentration of Pb^{2+}

The effect of the Pb^{2+} initial concentration on the removal efficiency and adsorption capacity of MCB and CB is shown in Fig. 10. When the initial concentration of Pb^{2+} increased from 10 to 300 mg/L, the adsorption capacity of MCB increased from 9.53 to 177.23 mg/g, and the removal rate decreased from 100% to 72.91%, while the removal rate of CB decreased to 58.29% and adsorption quantity increased from 9 to 160.9 mg/g. Given a certain dosage of MCB and CB, the availability of adsorption sites was better at a low Pb^{2+} concentration and led to an increase in the removal rate and adsorption quantity. Previous studies indicated the promising removal potential of biochar with multiple heavy metals in an aqueous environment [25–28], the removal performance of MCB with multiple heavy metals will be investigated in the future study. In the other hands, the heavy metals retained by the biochar was difficult to be desorbed, making the used sorbent material hazardous wastes if not well-disposed of under natural conditions [72]. According to the literature, the recycle method of heavy metals contained biochar including that elution generation, capacitors materials, and catalysts or catalysts carrier. Poonam et al. [73] found that heavy metals were efficiently desorbed from the saturated biochar, achieving approximately 90% regeneration by elution with 0.1 M HNO_3 . Wang et al. [74] reported that the carbon materials produced a supercapacitor electrode. Shen et al. [75] showed that the magnetic biochar can be used as catalysts or catalysts carrier. Therefore, the re-usability of MCB and CB should take

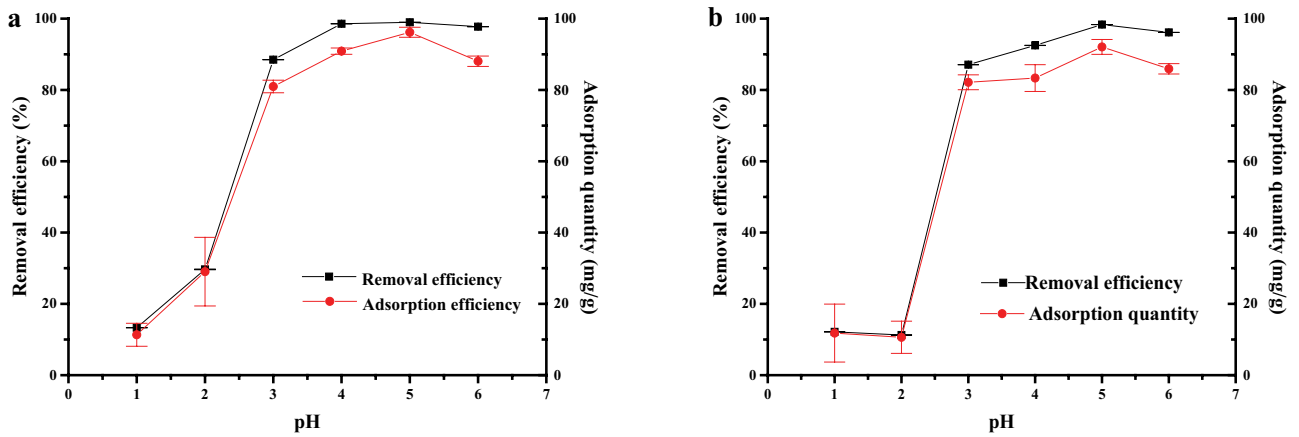


Fig. 8. Effect of solution pH on the removal efficiency and adsorption capacity of Pb²⁺. (a) MCB and (b) CB (dosage: 1 g/L; initial Pb²⁺ concentration: 100 mg/L; temperature: 298 K; time: 6 h).

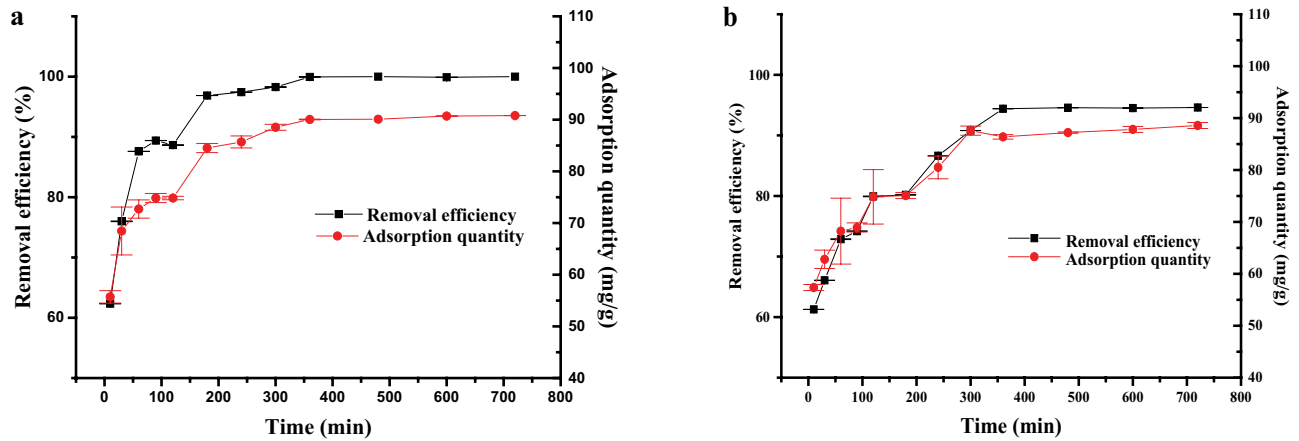


Fig. 9. Effect of contact time on the removal efficiency and adsorption capacity of Pb²⁺. (a) MCB and (b) CB (dosage: 1 g/L; initial Pb²⁺ concentration: 100 mg/L; temperature: 298 K; initial pH: 5).

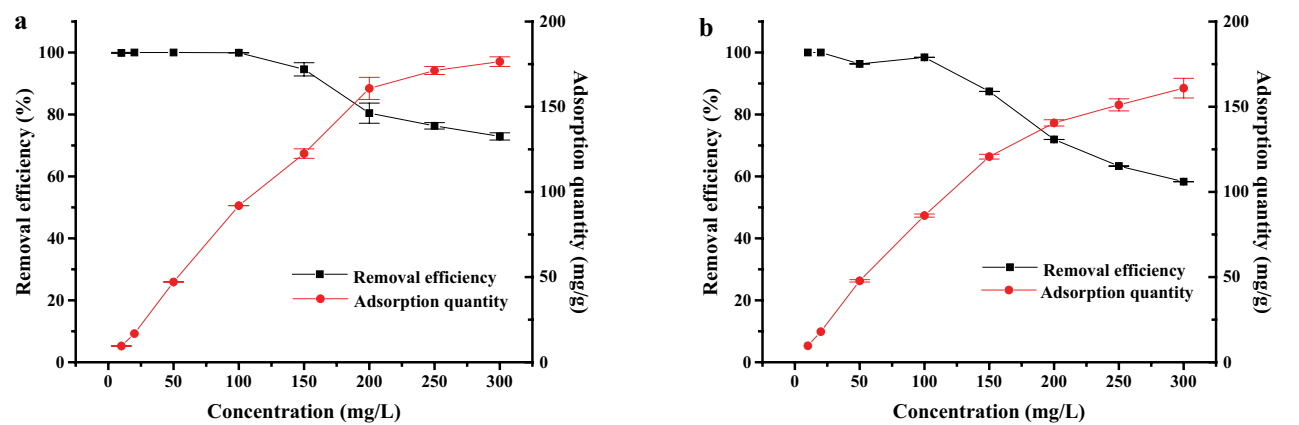


Fig. 10. Effect of the initial concentration (Pb²⁺) on the removal efficiency and adsorption capacity of Pb²⁺. (a) MCB and (b) CB (dosage: 1 g/L; temperature: 298 K; time: 6 h; initial pH: 5).

into consideration in future study regarding the practical application.

3.6. Effect of temperature

The effects of temperature on Pb²⁺ removal is shown in Fig. 11. When the temperature increased from 288 to 303 K, the overall adsorption capacity of Pb²⁺ decreased. The removal rate of MCB decreased from 97% to 79%, whilst the adsorption quantity decreased from 92 to 82 mg/g. The removal efficiency of CB decreased from 88% to 65%, and the adsorption quantity decreased from 84 to 66 mg/g. The removal efficiency and adsorption quantity decreased with increasing temperature, indicating the dominance of the exothermic process of adsorption [76]. These results showed that MCB and CB can better adsorb Pb²⁺ at low temperatures, indicating high energy efficiency and a consequent cost reduction for practical applications.

3.7. Adsorption kinetics

The adsorption kinetics were analyzed using the pseudo-first-order, pseudo-second-order, and diffusion equation models. The kinetics data of MCB and CB are shown in Tables 1 and 2. By comparing the similarity between the experimental and calculated values, the pseudo-second-order model provided the best description of the adsorption process, with a higher coefficient of MCB ($R^2 = 0.9994$) and CB ($R^2 = 0.9986$). This indicates that chemical adsorption is the rate-limiting factor for the adsorption of Pb²⁺ by MCB and CB [5,76].

3.8. Adsorption isotherm

The adsorption isotherms of adsorption analyzed based on the data are summarized in Tables 3 and 4. The Langmuir adsorption model accurately illustrated the adsorption process, with the higher coefficient fitting

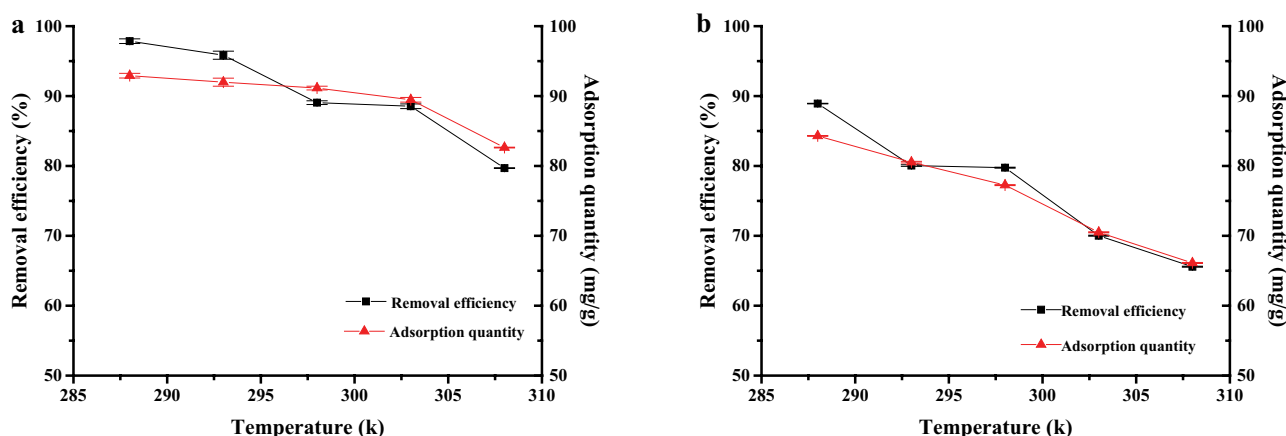


Fig. 11. Effect of temperature on the removal efficiency and adsorption capacity of Pb²⁺. (a) MCB and (b) CB (dosage: 1 g/L; initial Pb²⁺ concentration: 100 mg/L; time: 6 h; initial pH: 5).

Table 1
Kinetic parameters of the pseudo-first, pseudo-second, and intraparticle diffusion models of the adsorption of Pb²⁺ by CB

Concentration (mg/L)	Q_{exp} (mg/g)	Pseudo-first-order			Pseudo-second-order			Intraparticle diffusion		
		k_1 (min ⁻¹)	Q_e (mg/g)	R^2	k_2 (min ⁻¹)	Q_e (mg/g)	R^2	k_p (mg/g/min ^{1/2})	C (mg/g)	R^2
100	88.57	0.0068	30.71	0.8775	0.0005	90.91	0.9986	0.0813	66.3	0.7567
200	145.89	0.007	100.2	0.9425	0.0001	153.85	0.9926	0.2223	82.946	0.7947
300	168.08	0.0063	107.52	0.9344	0.0001	178.57	0.9903	0.2485	96.389	0.8655

Table 2
Kinetic parameters of the pseudo-first, pseudo-second, and intraparticle diffusion models of the adsorption of Pb²⁺ by MCB

Concentration (mg/L)	Q_{exp} (mg/g)	Pseudo-first-order			Pseudo-second-order			Intraparticle diffusion		
		k_1 (min ⁻¹)	Q_e (mg/g)	R^2	k_2 (min ⁻¹)	Q_e (mg/g)	R^2	k_p (mg/g/min ^{1/2})	C (mg/g)	R^2
100	90.79	0.0094	36.92	0.9732	0.0006	92.59	0.9994	0.0784	70.148	0.664
200	156.75	0.0089	104.42	0.9595	0.0002	163.93	0.9974	0.2075	100.39	0.7402
300	185.08	0.0067	123.85	0.9588	0.0001	196.08	0.9927	0.2745	106.65	0.8479

Table 3
Langmuir, Freundlich, and Dubinin–Radushkevich models and correlation coefficients for the adsorption of Pb²⁺ by CB

Temperature (K)	Langmuir model			Freundlich model			Dubinin–Radushkevich model			
	Q_m (mg/g)	K_L (L/mg)	R^2	$1/n$	$K_f^{1/n}$ (mg/g)	R^2	β (mol ² /J ²)	Q_m (mg/g)	E (kJ/mol)	R^2
288	156.25	0.3575	0.9966	0.2259	2.3843	0.8065	2×10^{-8}	140.04	6.25	0.9344
298	156.25	0.5926	0.9955	0.2460	2.7114	0.8362	2×10^{-8}	120.99	12.5	0.8759
308	128.21	0.3529	0.9908	0.2659	2.8351	0.7458	4×10^{-8}	112.98	12.5	0.9540

Table 4
Langmuir, Freundlich, and Dubinin–Radushkevich models and correlation coefficients for the adsorption of Pb²⁺ by MCB

Temperature (K)	Langmuir model			Freundlich model			Dubinin–Radushkevich model			
	Q_m (mg/g)	K_L (L/mg)	R^2	$1/n$	$K_f^{1/n}$ (mg/g)	R^2	β (mol ² /J ²)	Q_m (mg/g)	E (kJ/mol)	R^2
288	208.33	0.8571	0.9992	0.3457	3.8832	0.9515	3×10^{-8}	154.62	12.5	0.9520
298	192.31	0.4094	0.991	0.3504	3.9501	0.8886	4×10^{-8}	130.67	6.25	0.9189
308	175.44	0.7403	0.9977	0.3239	3.9802	0.8745	2×10^{-8}	117.52	8.33	0.8273

of MCB ($R^2 = 0.9992$) and CB ($R^2 = 0.9966$). This indicates that adsorption was dominated by a monolayer adsorption process, and the maximum monolayer adsorption capacities (Q_m) of MCB and CB onto Pb²⁺ was 208.33 and 156.25 mg/g, respectively. According to the characteristic analysis, the significantly high adsorption efficiency of MCB could be attributed to a discrepancy in the pore size structure and the surface groups due to the magnetic modification. In contrast, the maximum lead adsorption of MCB was higher than for some other adsorbents, such as; the KMnO₄ modified magnetic rice husk biochar (148 mg/g) [50], novel biochar loaded with nanoparticles (146.84 mg/g) [53], and the KMnO₄ treated hickory wood biochar (153.1 mg/g) [77]. In addition, as with the results from the temperature experiment, the adsorption capacity decreased with increasing temperature, thus confirming that the adsorption process can occur spontaneously at room temperature.

3.9. Adsorption thermodynamics

The thermodynamic data are shown in Table 5. The negative ΔG° was indicative of the spontaneous adsorption process. The negative value of ΔH° indicated the dominance of the exothermic reaction, which is consistent with the results of the temperature experiment. The negative ΔS° represented the decrease in system randomness [78], and according to the Gibbs free energy equation ($\Delta G^\circ = \Delta H^\circ - T\Delta S^\circ$), and given the negative value of entropy change, the value of

Gibbs free energy remained negative within a low temperature range. This revealed that the adsorption of Pb²⁺ by MCB and CB was a spontaneous exothermic process at relative low temperature scale, contributing to low energy consumption and beneficial to cost reduction of the practical application.

4. Conclusion

The magnetic MCB was successfully fabricated via one-step method. The SEM image revealed the structural difference between the two biochar, with MCB characterized by a more porous honeycomb structure than that of CB. The specific surface area of MCB and CB was determined as 613.69 and 356.68 m²/g, respectively. FTIR analysis indicated that the metal oxide and hydroxide groups were only present on the surface of MCB, and that functional groups of O–H, C=O, and C≡C were present in both MCB and CB. Further, XRD indicated the presence of Fe₃C in the MCB. The maximum monolayer adsorption capacity (Q_m) of MCB and CB onto Pb²⁺ reached 208.33 and 156.25 mg/g, respectively. The pseudo-second-order model was identified as a more suitable kinetic model for MCB and CB, with a higher coefficient ($R^2 > 0.99$). The adsorption isotherms were well-described by the Langmuir adsorption model ($R^2 > 0.99$), indicating the dominance of monolayer adsorption. The thermodynamics of Pb²⁺ by MCB and CB was found to be a spontaneous exothermic process in the low-temperature range. In conclusion, this study demonstrated that magnetic

Table 5
Adsorption thermodynamics parameters of the adsorption of Pb²⁺ by MCB and CB at different temperatures

	Ln k_e			ΔG° (kJ/mol)			ΔH° (kJ/mol)	ΔS° (J/mol) k
	288 K	298 K	308 K	288 K	298 K	308 K		
MCB	4.87	5.02	4.28	−12.47	−12.02	−10.60	−2.57	−3.91
CB	4.56	4.04	4.05	−11.30	−10.35	−9.70	−2.29	−3.46

modification could enhance heavy metal removal efficiency and indicates that MCB is a promising Pb^{2+} adsorbent, which has a high adsorption efficiency and is easily affordable.

Acknowledgments

This work was supported by Key Research and Development Program of Shandong Province, PR China (2019GSF109103), Distinguished Middle-Aged and Young Scientist Encourage and Reward Foundation of Shandong Province (ZR2016CB18), Project of Shandong Province Higher Educational Science and Technology Program (No. J18KA186), National Natural Science Foundation of China (No. 51708340), International Postdoctoral Exchange Fellowship Program (No. 20180063), Special Financial Grant from the China Postdoctoral Science Foundation (No. 2015T80738), and National Major Science and Technology Program for Water Pollution Control and Treatment (2017ZX07101001).

References

- [1] J.R. Bacon, N.S. Dinev, Isotopic characterisation of lead in contaminated soils from the vicinity of a non-ferrous metal smelter near Plovdiv, Bulgaria, *Environ. Pollut.*, 134 (2005) 247–255.
- [2] V. Ettler, M. Mihaljevič, M. Komárek, ICP-MS measurements of lead isotopic ratios in soils heavily contaminated by lead smelting: tracing the sources of pollution, *Anal. Bioanal. Chem.*, 378 (2004) 311–317.
- [3] M.M. Matlock, B.S. Howerton, D.A. Atwood, Chemical precipitation of lead from lead battery recycling plant wastewater, *Ind. Eng. Chem. Res.*, 41 (2002) 1579–1582.
- [4] Y.-F. Zhang, Z.-L. Xu, Study on the treatment of industrial wastewater containing Pb^{2+} ion using a coupling process of polymer complexation-ultrafiltration, *Sep. Sci. Technol.*, 38 (2003) 1585–1596.
- [5] A. Supong, P.C. Bhomick, M. Baruah, C. Pongener, U.B. Sinha, D. Sinha, Adsorptive removal of bisphenol a by biomass activated carbon and insights into the adsorption mechanism through density functional theory calculations, *Sustainable Chem. Pharm.*, 13 (2019) 100159, doi: 10.1016/j.scp.2019.100159.
- [6] F. Xu, D.-l. Ouyang, E.R. Rene, H.Y. Ng, L.-l. Guo, Y.-j. Zhu, L.-l. Zhou, Q. Yuan, M.-s. Miao, Q. Wang, Q. Kong, Electricity production enhancement in a constructed wetland-microbial fuel cell system for treating saline wastewater, *Bioresour. Technol.*, 288 (2019) 121462, doi: 10.1016/j.biortech.2019.121462.
- [7] S. Tong, Y.E.v. Schirnding, T. Prapamontol, Environmental lead exposure: a public health problem of global dimensions, *Bull. World Health Organ.*, 78 (2000) 1068–1077.
- [8] O.A. Ramirez, O.M. Abdeldayem, A. Pugazhendhi, E.R. Rene, Current updates and perspectives of biosorption technology: an alternative for the removal of heavy metals from wastewater, *Curr. Pollut. Rep.*, 6 (2020) 8–27.
- [9] E. Suhartono, Y.W. Ulfarini, T. Triawanti, W.A. Mustaqim, R.T. Firdaus, M.H.M. Setiawan, Increased bone calcium dissociation in lead-exposed rats, *Universa Med.*, 31 (2015) 151–158.
- [10] E. Baker, P. Landrigan, A. Barbour, D. Cox, D. Folland, R. Ligo, J. Throckmorton, Occupational lead poisoning in the United States: clinical and biochemical findings related to blood lead levels, *Occup. Environ. Med.*, 36 (1979) 314–322.
- [11] L. Gerhardsson, D.R. Chettle, V. Englyst, G.F. Nordberg, H. Nyhlin, M.C. Scott, A.C. Todd, O. Vesterberg, Kidney effects in long term exposed lead smelter workers, *Br. J. Ind. Med.*, 49 (1992) 186–192.
- [12] A. Kumar, P.K. Dey, P.N. Singla, R.S. Ambasht, S.K. Upadhyay, Blood lead levels in children with neurological disorders, *J. Trop. Pediatr.*, 44 (1998) 320–322.
- [13] B. Somashekaraiah, B. Venkaiah, A. Prasad, Biochemical diagnosis of occupational exposure to lead toxicity, *Bull. Environ. Contam. Toxicol.*, 44 (1990) 268–275.
- [14] P.C. Mishra, R.K. Patel, Removal of lead and zinc ions from water by low cost adsorbents, *J. Hazard. Mater.*, 168 (2009) 319–325.
- [15] EPB, Environmental quality Standards for Surface Water (GB 3838–2002), Environmental Protection Bureau, Beijing, 2002.
- [16] L. Singh Thakur, Heavy metal Cu, Ni and Zn: Toxicity, health hazards and their removal techniques by low cost adsorbents: a short overview, *Int. J. Plant. Sci.*, 3 (2013) 143–157.
- [17] M. Naushad, Surfactant assisted nano-composite cation exchanger: development, characterization and applications for the removal of toxic Pb^{2+} from aqueous medium, *Chem. Eng. J.*, 235 (2014) 100–108.
- [18] A.A.H. Faisal, S.F.A. Al-Wakel, H.A. Assi, L.A. Naji, M. Naushad, Waterworks sludge-filter sand permeable reactive barrier for removal of toxic lead ions from contaminated groundwater, *J. Water Process. Eng.*, 33 (2020) 101112, doi: 10.1016/j.jwpe.2019.101112.
- [19] M. Naushad, A. Mittal, M. Rathore, V. Gupta, Ion-exchange kinetic studies for Cd(II), Co(II), Cu(II), and Pb(II) metal ions over a composite cation exchanger, *Desal. Water Treat.*, 54 (2015) 2883–2890.
- [20] D. Lakherwal, Adsorption of heavy metals: a review, *Int. J. Environ. Res. Dev.*, 4 (2014) 41–48.
- [21] K.Y. Foo, B.H. Hameed, An overview of landfill leachate treatment via activated carbon adsorption process, *J. Hazard. Mater.*, 171 (2009) 54–60.
- [22] S.M. Yakout, A.E.H.M. Daifullah, S.A. El-Reefy, Pore structure characterization of chemically modified biochar derived from rice straw, *Environ. Eng. Manage. J.*, 14 (2015) 473–480.
- [23] W. Gwenz, N. Chaukura, C. Noubactep, F.N.D. Mukome, Biochar-based water treatment systems as a potential low-cost and sustainable technology for clean water provision, *J. Environ. Manage.*, 197 (2017) 732–749.
- [24] M. Ahmad, A.U. Rajapaksha, J.E. Lim, M. Zhang, N. Bolan, D. Mohan, M. Vithanage, S.S. Lee, Y.S. Ok, Biochar as a sorbent for contaminant management in soil and water: a review, *Chemosphere*, 99 (2014) 19–33.
- [25] M. Inyang, B. Gao, Y. Yao, Y. Xue, A.R. Zimmerman, P. Pullammanappallil, X. Cao, Removal of heavy metals from aqueous solution by biochars derived from anaerobically digested biomass, *Bioresour. Technol.*, 110 (2012) 50–56.
- [26] Y. Zhou, B. Gao, A.R. Zimmerman, J. Fang, Y. Sun, X. Cao, Sorption of heavy metals on chitosan-modified biochars and its biological effects, *Chem. Eng. J.*, 231 (2013) 512–518.
- [27] T.A. Saleh, M. Tuzen, A. Sari, Magnetic activated carbon loaded with tungsten oxide nanoparticles for aluminum removal from waters, *J. Environ. Chem. Eng.*, 5 (2017) 2853–2860.
- [28] R. Shan, Y. Shi, J. Gu, Y. Wang, H. Yuan, Single and competitive adsorption affinity of heavy metals toward peanut shell-derived biochar and its mechanisms in aqueous systems, *Chin. J. Chem. Eng.*, 28 (2020) 1375–1383.
- [29] B. Chen, Z. Chen, S. Lv, A novel magnetic biochar efficiently sorbs organic pollutants and phosphate, *Bioresour. Technol.*, 102 (2011) 716–723.
- [30] I. Šafařík, K. Nymburská, M. Šafaříková, Adsorption of water-soluble organic dyes on magnetic charcoal, *J. Chem. Technol.*, 69 (1997) 1–4.
- [31] G. Zhang, J. Qu, H. Liu, A.T. Cooper, R.J.C. Wu, $CuFe_2O_4$ /activated carbon composite: a novel magnetic adsorbent for the removal of acid orange II and catalytic regeneration, *Chemosphere*, 68 (2007) 1058–1066.
- [32] S. Liu, H.A. Wiatrowski, Reduction of Hg(II) to Hg(0) by magnetite from two magnetotactic bacterial, *Geomicrobiol. J.*, 43 (2009) 5307–5313.
- [33] N. Subedi, A. Lähde, E. Abu-Danso, J. Iqbal, A. Bhatnagar, A comparative study of magnetic chitosan ($Chi@Fe_3O_4$) and graphene oxide modified magnetic chitosan ($Chi@Fe_3O_4GO$) nanocomposites for efficient removal of Cr(VI) from water, *Int. J. Biol. Macromol.*, 137 (2019) 948–959.

- [34] M. Imran, Z.U.H. Khan, J. Iqbal, N.S. Shah, M. Rizwan, Potential of siltstone and its composites with biochar and magnetite nanoparticles for the removal of cadmium from contaminated aqueous solutions: batch and column scale studies, *Environ. Pollut.*, 259 (2020) 113938, doi: 10.1016/j.envpol.2020.113938.
- [35] D. Mohan, A. Sarswat, V.K. Singh, M. Alexandre-Franco, C.U. Pittman, Development of magnetic activated carbon from almond shells for trinitrophenol removal from water, *Chem. Eng. J.*, 172 (2011) 1111–1125.
- [36] M. Ahmad, S.S. Lee, X. Dou, D. Mohan, J.-K. Sung, J.E. Yang, Y.S. Ok, Effects of pyrolysis temperature on soybean stover- and peanut shell-derived biochar properties and TCE adsorption in water, *Bioresour. Technol.*, 118 (2012) 536–544.
- [37] N. Mahinpey, P. Murugan, T. Mani, R. Raina, Analysis of bio-oil, biogas, and biochar from pressurized pyrolysis of wheat straw using a tubular reactor, *Energy Fuel*, 23 (2009) 2736–2742.
- [38] A. Samsuri, F. Sadegh-Zadeh, B. Seh-Bardan, Characterization of biochars produced from oil palm and rice husks and their adsorption capacities for heavy metals, *Int. J. Environ. Sci. Technol.*, 11 (2014) 967–976.
- [39] J. Lu, C. Zhang, J. Wu, Y. Luo, Adsorptive removal of bisphenol A using N-doped biochar made of *Ulva prolifera*, *Water Air Soil Pollut.*, 228 (2017) 327, doi: 10.1007/s11270-017-3516-0.
- [40] N. Silanikove, Effect of CaO-OR NaOH-hydrogen peroxide treatments on the composition and *in-vitro* digestibility of cotton straw, *Bioresour. Technol.*, 48 (1994) 71–73.
- [41] M. Hussain, M. Imran, G. Abbas, M. Shahid, M. Iqbal, M.A. Naeem, B. Murtaza, M. Amjad, N.S. Shah, Z. Ul Haq Khan, A. Ul Islam, A new biochar from cotton stalks for As(V) removal from aqueous solutions: its improvement with H₃PO₄ and KOH, *Environ. Geochem. Health*, 42 (2019) 2519–2534.
- [42] Y.-d. Du, H.-q. Liu, L. Shu, Y. Feng, Q. Kong, F. Xu, Q. Wang, C.-c. Zhao, Adsorption of ofloxacin from aqueous solution using low-cost biochar obtained from cotton stalk, *Desal. Water Treat.*, 135 (2018) 372–380.
- [43] Z. Wang, H. Guo, F. Shen, G. Yang, Y. Zhang, Y. Zeng, L. Wang, H. Xiao, S. Deng, Biochar produced from oak sawdust by Lanthanum (La)-involved pyrolysis for adsorption of ammonium (NH₄⁺), nitrate (NO₃⁻), and phosphate (PO₄³⁻), *Chemosphere*, 119 (2015) 646–653.
- [44] L. GaParovi, Z. Koreňová, U. Jelemensky, Kinetic study of wood chips decomposition by TGA, *Chem. Pap.*, 64 (2010) 174–181.
- [45] I.I. Gurten, M. Ozmak, E. Yagmur, Z. Aktas, Preparation and characterisation of activated carbon from waste tea using K₂CO₃, *Biomass Bioenergy*, 37 (2012) 73–81.
- [46] K. Fu, Q. Yue, B. Gao, Y. Sun, L. Zhu, Preparation, characterization and application of lignin-based activated carbon from black liquor lignin by steam activation, *Chem. Eng. J.*, 228 (2013) 1074–1082.
- [47] A.-Y. Wang, K. Sun, L. Wu, P. Wu, W. Zeng, Z. Tian, Q.-X. Huang, Co-carbonization of biomass and oily sludge to prepare sulfamethoxazole super-adsorbent materials, *Sci. Total Environ.*, 698 (2020) 134238, doi: 10.1016/j.scitotenv.2019.134238.
- [48] R. Li, H. Deng, X. Zhang, J.J. Wang, M.K. Awasthi, Q. Wang, R. Xiao, B. Zhou, J. Du, Z. Zhang, High-efficiency removal of Pb(II) and humate by a CeO₂-MoS₂ hybrid magnetic biochar, *Bioresour. Technol.*, 273 (2019) 335–340.
- [49] Y. Zhao, R. Zhang, H. Liu, M. Li, T. Chen, D. Chen, X. Zou, R.L. Frost, Green preparation of magnetic biochar for the effective accumulation of Pb(II): performance and mechanism, *Chem. Eng. J.*, 375 (2019) 122011, doi: 10.1016/j.cej.2019.122011.
- [50] C. Sun, T. Chen, Q. Huang, J. Wang, S. Lu, J. Yan, Enhanced adsorption for Pb(II) and Cd(II) of magnetic rice husk biochar by KMnO₄ modification, *Environ. Sci. Pollut. Res.*, 26 (2019) 8902–8913.
- [51] F. Lian, G. Cui, Z. Liu, L. Duo, G. Zhang, B. Xing, One-step synthesis of a novel N-doped microporous biochar derived from crop straws with high dye adsorption capacity, *J. Environ. Manage.*, 176 (2016) 61–68.
- [52] Y.-n. Wang, Q. Liu, L. Shu, M.-s. Miao, Y.-z. Liu, Q. Kong, Removal of Cr(VI) from aqueous solution using Fe-modified activated carbon prepared from luffa sponge: kinetic, thermodynamic, and isotherm studies, *Desal. Water Treat.*, 57 (2016) 29467–29478.
- [53] C. Wang, H. Wang, Pb(II) sorption from aqueous solution by novel biochar loaded with nano-particles, *Chemosphere*, 192 (2018) 1–4.
- [54] Z. Huang, Q. Lu, J. Wang, X. Chen, X. Mao, Z. He, Inhibition of the bioavailability of heavy metals in sewage sludge biochar by adding two stabilizers, *PLoS One*, 12 (2017) e0183617, doi: 10.1371/journal.pone.0183617.
- [55] S. Muljani, B.W. Wahyudi, S. Suprihatin, K.J.R. Sumada, Synthesis of matrix Si-K-HAs gel from geothermal sludge and peat, *REAKTOR*, 18 (2018) 76–83.
- [56] Ö. Tamer, D. Avci, Y. Atalay, Quantum chemical characterization of N-(2-hydroxybenzylidene) acetohydrazide (HBAH): a detailed vibrational and NLO analysis, *Spectrochim. Acta, Part A*, 117 (2014) 78–86.
- [57] F.A. Lothfy, M.F. Haron, H.A. Rifaie, Fabrication and characterization of jackfruit seed powder and polyvinyl alcohol blend as biodegradable plastic, *J. Photopolym. Sci. Technol.*, 3 (2018) 1–5.
- [58] S. Liang, Y. Han, L. Wei, A.G. McDonald, Production and characterization of bio-oil and bio-char from pyrolysis of potato peel wastes, *Biomass Convers. Biorefin.*, 5 (2015) 237–246.
- [59] N. Prakongkep, R.J. Gilkes, W. Wiriyakitnatekul, Forms and solubility of plant nutrient elements in tropical plant waste biochars, *J. Plant Nutr. Soil Sci.*, 178 (2015) 732–740.
- [60] S. Zhang, L. Tao, M. Jiang, G. Gou, Z. Zhou, Single-step synthesis of magnetic activated carbon from peanut shell, *Mater. Lett.*, 157 (2015) 281–284.
- [61] J. Lu, C. Zhang, J. Wu, One-pot synthesis of magnetic algal carbon/sulfidated nanoscale zerovalent iron composites for removal of bromated disinfection by-product, *Chemosphere*, 250 (2020) 126257, doi: 10.1016/j.chemosphere.2020.126257.
- [62] C. Zhang, J. Lu, J. Wu, One-step green preparation of magnetic seaweed biochar/sulfidated Fe⁰ composite with strengthened adsorptive removal of tetrabromobisphenol A through *in situ* reduction, *Bioresour. Technol.*, 307 (2020) 123170, doi: 10.1016/j.biortech.2020.123170.
- [63] J. Iqbal, N.S. Shah, M. Sayed, M. Imran, N. Muhammad, F.M. Howari, S.A. Alkhoori, J.A. Khan, Z.U.H. Khan, A. Bhatnagar, Synergistic effects of activated carbon and nano-zerovalent copper on the performance of hydroxyapatite-alginate beads for the removal of As³⁺ from aqueous solution, *J. Cleaner Prod.*, 235 (2019) 875–886.
- [64] G.-X. Yang, H. Jiang, Amino modification of biochar for enhanced adsorption of copper ions from synthetic wastewater, *Water Res.*, 48 (2014) 396–405.
- [65] Z. Zhou, Y.-g. Liu, S.-b. Liu, H.-y. Liu, G.-m. Zeng, X.-f. Tan, C.-p. Yang, Y. Ding, Z.-l. Yan, X.-x. Cai, Sorption performance and mechanisms of arsenic(V) removal by magnetic gelatin-modified biochar, *Chem. Eng. J.*, 314 (2017) 223–231.
- [66] A. Mukherjee, A. Zimmerman, W. Harris, Surface chemistry variations among a series of laboratory-produced biochars, *Geoderma*, 163 (2011) 247–255.
- [67] A. Üçer, A. Uyanik, Ş. Aygün, Adsorption of Cu(II), Cd(II), Zn(II), Mn(II) and Fe(III) ions by tannic acid immobilised activated carbon, *Sep. Purif. Technol.*, 47 (2006) 113–118.
- [68] A. Maged, J. Iqbal, S. Kharbish, I.S. Ismael, A. Bhatnagar, Tuning tetracycline removal from aqueous solution onto activated 2:1 layered clay mineral: characterization, sorption and mechanistic studies, *J. Hazard. Mater.*, 384 (2020) 121320, doi: 10.1016/j.jhazmat.2019.121320.
- [69] H. Liu, F. Li, L. Chen, J. Ding, M. Sun, Adsorptive removal of Pb(II) ions with magnetic metal-organic frameworks from aqueous samples, *Gen. Chem.*, 3 (2017) 134–139.
- [70] K.-W. Jung, T.-U. Jeong, J.-W. Choi, K.-H. Ahn, S.-H. Lee, Adsorption of phosphate from aqueous solution using electrochemically modified biochar calcium-alginate beads: batch and fixed-bed column performance, *Bioresour. Technol.*, 244 (2017) 23–32.
- [71] B. Özkaya, Adsorption and desorption of phenol on activated carbon and a comparison of isotherm models, *J. Hazard. Mater.*, 129 (2006) 158–163.

- [72] L. Wang, Y. Wang, F. Ma, V. Tankpa, S. Bai, X. Guo, X. Wang, Mechanisms and reutilization of modified biochar used for removal of heavy metals from wastewater: a review, *Sci. Total Environ.*, 668 (2019) 1298–1309.
- [73] Poonam, B.S. Kumar, K. Narendra, Kinetic study of lead (Pb²⁺) removal from battery manufacturing wastewater using bagasse biochar as biosorbent, *Appl. Water Sci.*, 8 (2018) 119.
- [74] Y. Wang, Y. Wang, L. Jiang, Freestanding carbon aerogels produced from bacterial cellulose and its Ni/MnO₂/Ni(OH)₂ decoration for supercapacitor electrodes, *J. Appl. Electrochem.*, 48 (2018) 495–507.
- [75] Y. Shen, P. Zhao, Q. Shao, F. Takahashi, K. Yoshikawa, *In situ* catalytic conversion of tar using rice husk char/ash supported nickel-iron catalysts for biomass pyrolytic gasification combined with the mixing-simulation in fluidized-bed gasifier, *Appl. Energy*, 160 (2015) 808–819.
- [76] R.P. Mohubedu, P.N. Diagboya, C.Y. Abasi, E.D. Dikio, F. Mtunzi, Magnetic valorization of biomass and biochar of a typical plant nuisance for toxic metals contaminated water treatment, *J. Cleaner Prod.*, 209 (2019) 1016–1024.
- [77] H. Wang, B. Gao, S. Wang, J. Fang, Y. Xue, K. Yang, Removal of Pb(II), Cu(II), and Cd(II) from aqueous solutions by biochar derived from KMnO₄ treated hickory wood, *Bioresour. Technol.*, 197 (2015) 356–362.
- [78] V. Gupta, A. Mittal, L. Krishnan, V. Gajbe, Adsorption kinetics and column operations for the removal and recovery of malachite green from wastewater using bottom ash, *Sep. Purif. Technol.*, 40 (2004) 87–96.

Supplementary information

S1. Batch experiments

Adsorption capacity and removal rate of Pb²⁺ was expressed as:

$$Q_e = \frac{(C_0 - C_e)V}{M} \quad (1)$$

$$R = \frac{C_0 - C_e}{C_0} \times 100 \quad (2)$$

where Q_e (mg/g) was the equilibrium adsorption quantity, C_0 (mg/L) was the initial concentration of Pb²⁺, C_e (mg/L) was the equilibrium concentration of Pb²⁺, V (L) was the volume of the solution, M (g) was the mass of biochar, and R (%) was the removal rate of Pb²⁺.

S2. Adsorption kinetics

The pseudo-first-order model, pseudo-second-order model, and the diffusion equation model were expressed as

Pseudo-first-order model:

$$\ln(Q_e - Q_t) = \ln Q_e - k_1 t \quad (3)$$

Pseudo-second-order model:

$$\frac{t}{Q_t} = \frac{1}{k_2 Q_e^2} + \frac{1}{Q_e} t \quad (4)$$

The diffusion equation model:

$$Q_t = k_p t^{(1/2)} + C \quad (5)$$

where Q_t (mg/g) was the adsorption capacity of Pb²⁺ by biochar at t time, Q_e (mg/g) was the equilibrium adsorption capacity of Pb²⁺, k_1 , k_2 , and k_p were adsorption rate constant, and C was the constant.

S3. Adsorption isotherms

The Langmuir, Freundlich, and Dubinin–Radushkevich models were expressed as:

Langmuir model:

$$\frac{C_e}{Q_e} = \frac{1}{Q_m K_L} + \frac{1}{Q_m} C_e \quad (6)$$

Freundlich model:

$$\ln Q_e = \ln K_F + \frac{1}{n} \ln C_e \quad (7)$$

Dubinin–Radushkevich model:

$$\ln Q_e = \ln Q_m - \beta \varepsilon^2 \quad (8)$$

$$\varepsilon = RT \ln \left(1 + \frac{1}{C_e} \right) \quad (9)$$

$$E = (2\beta)^{-\frac{1}{2}} \quad (10)$$

where Q_e (mg/g) was the equilibrium adsorption capacity, C_e (mg/L) was the concentration of Pb²⁺ at equilibrium, Q_m (mg/g) was the maximum adsorption capacity of Pb²⁺, K_L was the Langmuir constant, K_F and n were the Freundlich constant, represents adsorption performance and adsorption strength, β was the adsorption energy correlation constant; R was the thermodynamic constant, T was the thermodynamic temperature, and E was the average adsorption free energy.

S4. Adsorption thermodynamic

The adsorption thermodynamic were expressed as:

$$\Delta G^\circ = -RT \ln k \quad (11)$$

$$\Delta G^\circ = \Delta H^\circ - T\Delta S^\circ \quad (12)$$

where R was the ideal gas constant (8.314 J/mol K), T was the thermodynamic temperature, k is the thermodynamic equilibrium constant, and obtained by multiplying Langmuir constant and Q_e .